Journal of Power Sources 516 (2021) 230658

Contents lists available at ScienceDirect

Journal of Power Sources

journal homepage: www.elsevier.com/locate/jpowsour

An experimental and modeling study of sodium-ion battery electrolytes

Kudakwashe Chayambuka [a,b,c,d], Ruth Cardinaels [e,a], Kevin L. Gering [f], L. Raijmakers [d], Grietus Mulder [b,c], Dmitri L. Danilov [a,d], Peter H.L. Notten [a,d,g,*]

[a] Eindhoven University of Technology, P.O. Box 513, 5600 MB, Eindhoven, the Netherlands
[b] VITO, Boeretang 200, 2400, Mol, Belgium
[c] EnergyVille, Thor Park 8310, 3600, Genk, Belgium
[d] Forschungszentrum Jülich, Fundamental Electrochemistry (IEK-9), D-52425, Jülich, Germany
[e] Soft Matter Rheology and Technology, Department of Chemical Engineering, KU Leuven, 3001, Leuven, Belgium
[f] Department of Biological & Chemical Processing, Idaho National Laboratory, Idaho Falls, ID, 83415-3732, USA
[g] Centre for Clean Energy Technology, University of Technology Sydney, Broadway, Sydney, NSW, 2007, Australia

HIGHLIGHTS

- Electrolyte conductivity and viscosity profiles of the $NaPF_6$ in EC and PC.
- Conductivity and viscosity results over a wide concentration and temperature range.
- The Advanced Electrolyte Model accurately predicts the experimental results.
- $NaPF_6$-based have higher conductivity compared to $LiPF_6$-based electrolytes.
- The cationic preferential ion solvation of EC correlates with electrode stability.

ARTICLE INFO

Keywords:
Sodium-ion battery
Electrolytes
Conductivity
Viscosity
Advanced electrolyte model

ABSTRACT

Electrolytes play an integral role in the successful operation of any battery chemistry. The reemergence of the sodium-ion battery (SIB) chemistry has therefore rejuvenated the search for optimized SIB salts and solvents. Recent experiments have found that 1 M $NaPF_6$ in ethylene carbonate (EC) and propylene carbonate (PC), $EC_{0.5}$: $PC_{0.5}$ (w/w) is the best binary electrolyte for SIBs. However, mathematical models, to elucidate these experimental findings, have so far been lacking. Furthermore, no attempts to understand the effect of EC composition on the conductivity and electrolyte stability have been performed. Herein, the viscosity and conductivity profiles of $NaPF_6$ in $EC_{0.5}$: $PC_{0.5}$ electrolyte are unraveled, using experimental and modeling approaches at different temperatures and salt concentrations. The viscosity is measured in a double-wall Couette cell and for the first time, the ionic conductivity is determined using two Pt blocking electrodes in a PAT-Cell electrochemical setup. Modeling is performed using the Advanced Electrolyte Model (AEM), a statistical mechanics software. It is shown that the conductivity and viscosity relationship follows a simple Stokes' law even at a low temperatures and high concentrations. In addition, the stability of binary and ternary electrolytes on hard carbon is shown to correlate with the preferential ion solvation of EC.

1. Introduction

Over the last decade, efforts to develop and commercialize sodium-ion batteries (SIBs) have been propelled by the supply shortage risk of lithium-ion battery (LIB) components and the need to avert overreliance on LIBs in emerging, large scale applications [1]. Several start-up companies have, in recent times, developed prototype SIB cells and successfully demonstrated comparable performance metrics to state-of-the-art LIBs [2–4]. In the aftermath of these achievements, SIBs have emerged as the most prominent "post lithium" energy storage technology, with the potential to complement and match the performances of LIBs in electric vehicles and grid energy storage applications.

In this battery chemistry transition endeavor, it is important to optimize SIB electrolytes and to elucidate their properties at different

* Corresponding author. Eindhoven University of Technology, P.O. Box 513, 5600 MB, Eindhoven, the Netherlands.
E-mail address: p.h.l.notten@tue.nl (P.H.L. Notten).

https://doi.org/10.1016/j.jpowsour.2021.230658
Received 29 March 2021; Accepted 16 October 2021
Available online 23 October 2021

concentrations and temperatures. This is because electrolytes play an essential role in several important performance metrics such as safety, rate capability, and electrode stability [5,6]. However, optimizing electrolyte properties is a nontrivial task given that binary, ternary and quaternary mixtures of solvents are necessary to obtain the optimal electrochemical stability window (ESW), ionic conductivity, viscosity, and thermal stability [5,6]. Blends of SIB electrolytes include solvents such as ethylene carbonate (EC), propylene carbonate (PC), dimethyl carbonate (DMC), 1,2 dimethoxyethane (DME), and diethyl carbonate (DEC) [7,8]. In addition, the commercial availability of battery-grade salts is often the crucial missing step in the development process of emerging battery chemistries [9]. As a result of the complexity involved, it is necessary to leverage modeling techniques as complementary tools, to speed-up the development and optimization of battery electrolytes.

One modeling strategy which has been highly successful is the statistical mechanics approach using the Advanced Electrolyte Model (AEM) created at the Idaho National Laboratory [10–13]. The AEM was developed by Gering for application in battery electrolytes and other electrolyte working fluids [12,13]. The success of the AEM originates from the provided fundamental understanding of solvation thermodynamics based on molecular level interactions between the solvent and ionic species [14]. This differs from the classical approach of solvation thermodynamics based on bulk macroscopic properties, such as viscosity and conductivity. The AEM has shown exceptional accuracy in predicting conductivity and viscosity properties of LIB electrolytes [10,11]. The AEM allows a wide selection and combination of the most common LIB and SIB salts and solvents, which include water, aprotic solvents, and room temperature ionic liquids. The AEM can be further used as an optimization tool for electrolytes of different compositions. Such optimization can enhance the SIB technology. For example, increasing the ionic conductivity and ESW would allow thicker electrode coatings and high voltage cells [15,16]. These strategies can significantly increase the energy density and reduce the manufacturing costs of batteries [17].

Although the $EC_{0.5}$: $PC_{0.5}$ (w/w) solvent has been identified as the most attractive for SIB application because of its high thermally stability and wide ESW [7], it is equally important to elucidate its extensive parameters such as viscosity and conductivity as a function of temperature and salt concentration, for application in electrochemical battery models. Herein, the SIB electrolytes composed of $NaPF_6$ salt and $EC_{0.5}$: $PC_{0.5}$ (w/w) binary solvent is investigated by experimental and modeling techniques. Properties of conductivity and viscosity are measured experimentally over a concentration and temperature range of 0–2 mol kg^{-1} and −10 to 50 °C, respectively, and the results are compared to the AEM predictions. Based on the experimental and AEM results, it is herein shown that the conductivity and viscosity relationship for the $EC_{0.5}$: $PC_{0.5}$ electrolyte, follows a simple Stokes' law. This demonstrates that ion pairing effects in the liquid organic electrolyte remain low over the concentration and temperature range studied and validates the use of the dilute solution theory in electrochemical models of this SIB electrolyte.

In this work, the experimental conductivity is determined using electrochemical impedance spectroscopy (EIS) on two Pt blocking electrodes in an El-Cell, PAT-Cell electrochemical setup. The electrolyte viscosity is determined in a double-wall Couette cell, which allows for a low volume of electrolytes and constant temperature control. The agreement between the AEM model results and experimental results for the $EC_{0.5}$: $PC_{0.5}$ solvent validates the experimental techniques and allows further optimization of the conductivity of the EC_x : PC_{1-x} solvent by tuning the EC composition. It is shown that the optimum EC composition varies with temperature and is governed by competing viscosity and ion pairing effects. Finally, comparing Li- and Na-based electrolytes reveals that Na-based electrolytes have a higher conductivity at high salt concentrations. These results encourage the exploration of highly concentrated SIB electrolytes, which have improved safety and charge transfer kinetics [18,19].

2. Theoretical background for conductivity measurements

Electrolyte conductivity can be measured from the impedance response of two identical blocking electrodes separated by the electrolyte. The two blocking electrodes are electrochemically inert electrodes which behave like an ideal capacitor upon polarization. The impedance response of such a blocking circuit is given by [20].

$$Z(\omega) = j\omega L + R_e + \frac{1}{(j\omega)^{\alpha} Q}\,, \tag{1}$$

where Z is the total impedance [Ω], j the imaginary unit, ω the frequency of the applied alternating signal [Hz], L the inductance due to, for example, the cable connections [H], and R_e the ionic resistance in the (bulk) electrolyte [Ω]. The frequency independent parameters α and Q are associated with a constant phase element (CPE), which accounts for the non-ideal capacitive response of the system [21]. Three possible scenarios of the CPE are as follows: (i) $\alpha = 1$, the impedance response is akin to that of a pure capacitor and Q represents the double layer capacitance (Q_{dl}) [F m^{-2}]. (ii) $\alpha = 0$, the impedance response is similar to that of a pure resistor, and (iii) $0 < \alpha < 1$, the impedance response shows local capacity dispersion due to electrode surface heterogeneity [20–22].

Fig. 1a illustrates an ionic conducting electrolyte in contact with two blocking electrodes and corresponding series inductor-resistor-capacitor equivalent circuit. Fig. 1b shows the complex impedance plane (Nyquist plot) measured with the blocking electrode setup and modeled with Eq. (1). At low ω, the imaginary component of the impedance approaches $-\infty$, meaning direct current flow is blocked in the low-frequency limit. As ω increases, the imaginary component of the impedance approaches zero. In the equivalent circuit model, $L = 0$ because the experimental data does not intersect with the real axis at high ω (see the inset in Fig. 1b). R_e can thus be determined from the intercept with the real axis in the Nyquist plot. In an ideal system wherein $\alpha = 1$, a vertical line is observed in the Nyquist plot. Nevertheless, in real practical systems, $\alpha \neq 1$ and a sloping line is observed due to the CPE.

The Nyquist plot is, however, not an accurate sequential graphical method to determine R_e, because the data is not linear at high frequencies and an intercept with the real axis can also observed at high frequencies (due to cable inductance for example). Instead, a Bode plot of the modulus of the admittance *versus* ω can separate R_e from the inductive artefacts [23]. The admittance Y [S] is defined as the inverse of the impedance

$$Y(\omega) = \frac{1}{Z(\omega)} = \frac{Z'}{|Z|^2} - j\frac{Z''}{|Z|^2}\,, \tag{2}$$

where Z' and Z'' are the real and imaginary parts of the impedance, respectively [Ω]. The modulus of the admittance, Y_{mod} [Ω] is then calculated as

$$Y_{mod} = \frac{1}{\sqrt{Z'^2 + Z''^2}}. \tag{3}$$

By fitting the impedance response of the model in Eq. (1) to the experimental EIS data in a Bode plot of Y_{mod}*versus* ω, accurate values of R_e can thus be determined. Fig. 1c illustrates the fitting of the equivalent circuit model shown in Eq. (1) to the experimental data in the Bode plot of Y_{mod} *versus*. ω . The model parameters are therefore determined in Fig. 1c and further verified in the Nyquist plot (Fig. 1b).

The ionic conductivity σ [$S\,m^{-1}$] can finally be deduced from R_e by

$$\sigma = \frac{K_{cell}}{R_e} \tag{4}$$

where K_{cell} is the cell constant [m^{-1}]. K_{cell} is determined using solutions of known conductivity (standard conductivity solutions) and depends on the blocking electrode surface area, the distance between the electrodes,

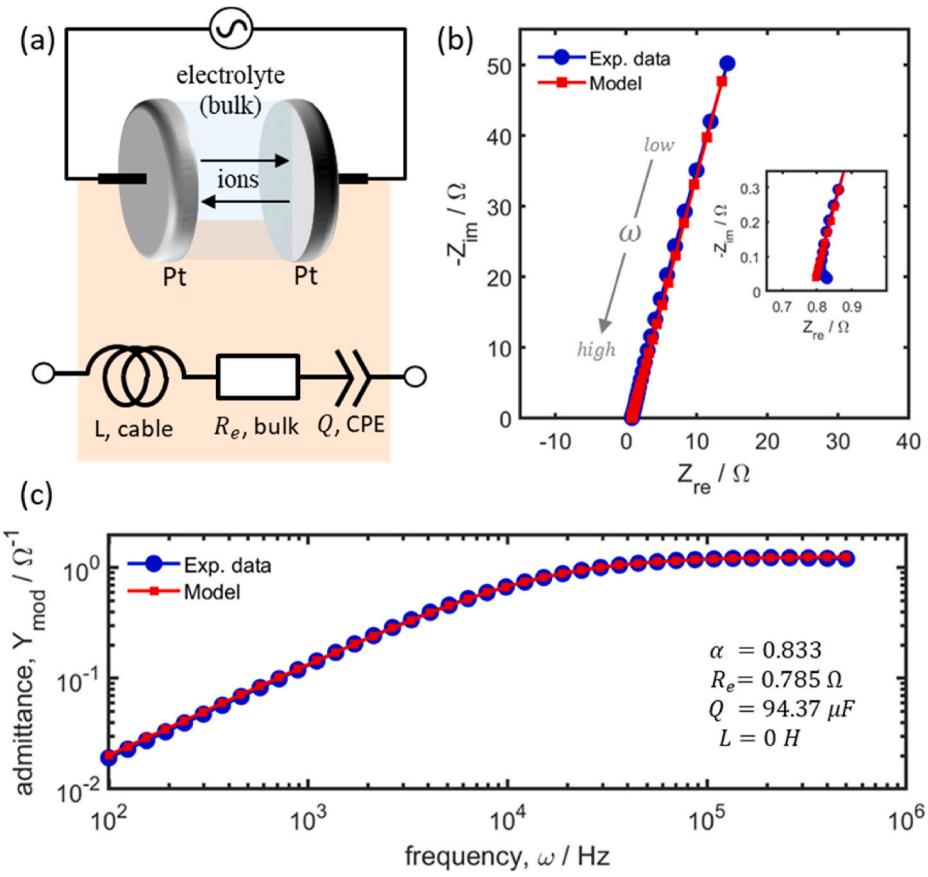

Fig. 1. Schematic representation of a blocking electrode measurement set-up and corresponding equivalent circuit (a). Nyquist plot of the impedance response of two blocking disk electrodes separated by an electrolyte and inset showing data near the high frequency intercept with the real axis (b). Bode plot of the modulus of admittance *versus* frequency (c). Typical experimental (blue) and model optimization results (red) obtained in this work are shown in (b) and (c). (For interpretation of the references to color in this figure legend, the reader is referred to the Web version of this article.)

and the tortuosity of the separator between the electrodes, if present.

3. Experimental

3.1. Preparation of electrolytes

An aprotic binary solvent mixture, consisting of 50 wt% ethylene carbonate (EC, Aldrich, anhydrous, 99.0%) and 50 wt% propylene carbonate (PC, Aldrich, anhydrous, 99.0%), was used for the conductivity and viscosity experiments. The $EC_{0.5}$: $PC_{0.5}$ (w/w) solvent was prepared at 60 °C, in order to melt and dissolve the EC. This procedure was carried out in an Argon filled glove box (Innovative Technology, Inc. Newburyport, MA), with controlled moisture and oxygen content. For the evaluation of viscosity and conductivity at different salt concentrations, $NaPF_6$ (Kishida, anhydrous, 99.0%) was dissolved in the $EC_{0.5}$: $PC_{0.5}$ solvent, to make concentrations of 0.15, 0.5, 1, 1.5 and 2 m (mol kg^{-1} of solvent). The molality scale is experimentally most convenient because the electrolyte volume varies with the amount of salt and

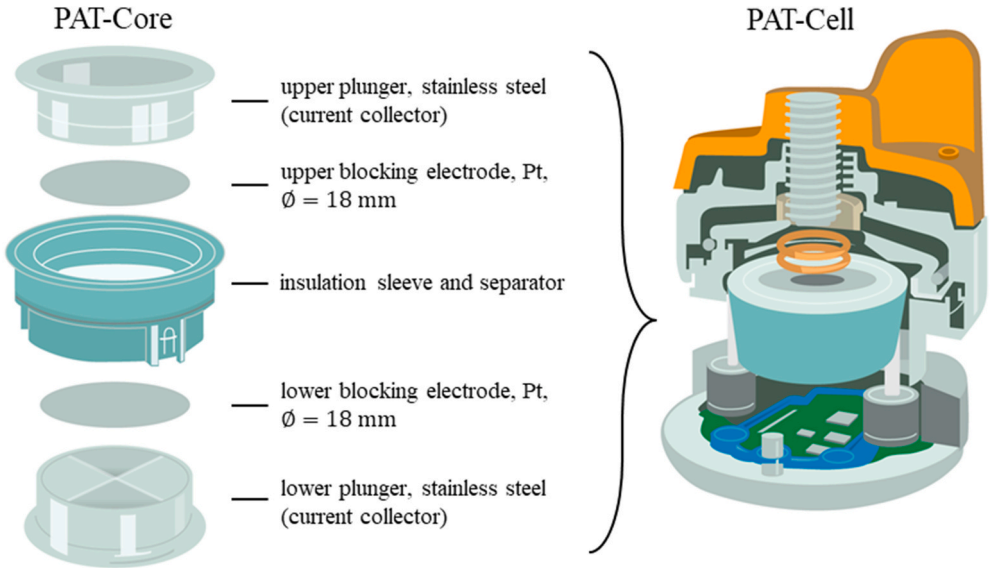

Fig. 2. Configuration of the PAT-Core and EL-Cell PAT-Cell used for the EIS electrolyte conductivity measurements. Adapted with permission [24].

temperature. In addition, salt concentrations are defined on the molality scale in the AEM software and corresponding molarity values are provided for comparison. All electrolytes and salts were used as-received.

3.2. Conductivity measurements

Electrolyte conductivities were measured in a hermetically-sealed PAT-Cell (EL-Cell GmbH, Hamburg, Germany) using EIS measurements on two Pt blocking electrodes, in the frequency range of 500–0.1 kHz using 40 logarithmically spaced frequencies. EIS measurements were performed in the potentiostatic mode using an amplitude of 10 mV (Autolab PGSTAT302 N).

Fig. 2 shows the PAT-Core mounted in the PAT-Cell used for the conductivity measurements. The PAT-Cell consists of an inner core, the PAT-Core, wherein two Pt discs (EL-Cell GmbH, $\varnothing = 18$ mm, Pt > 99.0%) were used as blocking electrodes, and two stainless-steel upper and lower plungers (EL Cell GmbH, 316L) were used as current collectors. The electrodes were separated by a 25 μm thick separator (EL Cell GmbH, Freudenberg Viledon). A polypropylene insulation sleeve was used to keep the electrodes, separator, and current collectors in place and thus seal the PAT-Core. To evaluate the cell constant, 1 mM KCl conductance standard solution (Aldrich, 99.0%) was used as electrolyte in the PAT-Cells, and the EIS measurements were repeated 7 times on different cell assemblies at 25 °C. An average cell constant of 0.9882 m^{-1} was determined with an accuracy of ± 3 % (based on standard error calculations).

All PAT-Cells, except for the KCl conductance standard test cells, were assembled and hermetically sealed in an argon-filled glove box. After sealing, the cells were taken out of the glove box and placed in a temperature chamber (Maccor, MTC-010). Inside the temperature chamber, the temperature was automatically set from − 10 to 50°C (10 °C steps). Each isothermal step was maintained for a total period of 5 h, and the EIS measurements were repeated at hourly intervals. The sealing of the PAT-Cells thus ensured stable measurements of the volatile electrolyte over a wide temperature range.

3.3. Viscosity measurements

The dynamic viscosity characterization of the $EC_{0.5} : PC_{0.5}$ (w/w) electrolyte at $NaPF_6$ concentrations of 0, 0.15, 0.5, 1, 1.5, and 2 mol kg^{-1} was performed, using a rotational rheometer with a Peltier temperature control unit. The rheometer (Anton Paar GmbH, MCR501) was configured and controlled via Rheoplus (software version 3.62). The temperature was set between −10 and 50 °C (10 °C steps). . At each temperature step, a waiting time of 20 min was required for the electrolyte temperature to reach steady-state. Due to the low viscosity and low volume constraints of the electrolyte samples, a double-wall Couette cell measuring system (Anton Paar, DIN 54453) was selected, in order to maximize the torque resolution for low volume electrolytes. In addition, a solvent trap system consisting of a pure $EC_{0.5} : PC_{0.5}$ solvent was used to minimize electrolyte evaporation from the cell during the tests and to limit the electrolyte-air contact. The solvent trap system works by creating a saturated solvent atmosphere in the cell [25].

Viscosity *versus* time curves were thus obtained at shear rates of 10, 100 and 1000 s^{-1}. Each shear rate was applied to the sample for a duration of 60 s with a sampling time of 1 s. All surfaces coming in contact with the electrolytes were thoroughly cleaned before measurements, first with deionized water and then with acetone, and left to dry in ambient air. An empty cell torque for the setup was determined, a parameter which was dominated by the solvent trap friction. An electrolyte volume of 3.8 mL was added to the cell, and the aforementioned shear rates were applied. Thixotropy was checked by the successive execution of two shear rate sweeps. The hysteresis between viscosity curves obtained with increasing *versus* decreasing shear rate was negligible, thus proving the absence of thixotropy. Moreover, the viscosity values did not depend on the applied shear rate, thereby demonstrating the Newtonian flow behavior of the electrolyte samples. At the shear rate of 1000 s^{-1} for example, a sample torque ranging between 0.2 and 30 mNm was obtained at the different temperatures and salt concentrations. By taking the average cell torque from the 3 shear rates, the electrolyte sample torque was finally calculated from the difference between the average cell torque and the empty cell torque.

3.4. AEM calculations

The AEM version 2.19.1 used in this work contains a graphic user interface and a library of 39 solvents and 28 salts. Specific details of the AEM methodology can be found in the following dedicated literature [12,13]. The user has an option to select a mixed electrolyte of up to 5 solvents and 2 salts. For the comparison between experimental and model results, in terms of viscosity and conductivity predictions at different temperature and concentration conditions, the $EC_{0.5} : PC_{0.5}$ (w/w) solvent and $NaPF_6$ salt were selected. The salt concentration range of 0 to 3 mol kg^{-1} was specified in combination with a temperature range of −10 to 50 °C (5 °C steps). The software gives 5 or 10 °C step options, and the former offers a finer grid and better fidelity in the Arrhenius calculations. In the input method for handling triple ion stability, the option $[ABA^+] = [BAB^-]$was selected. Finally, the Surface-Charge Attenuated Electrolyte Permittivity (SCAEP) and electrochemical double-layer calculations were not included. For the above calculations, the AEM does not require sophisticated computational power. Results are available in a few seconds on a standard desktop computer.

In order to compare properties of Na-based and Li-based electrolytes, AEM calculations were performed by selecting $EC_{0.5} : PC_{0.5}$ (w/w) solvent and $LiPF_6$ salt in the concentration and temperature range of 0 to 3 mol kg^{-1} and −10 to 50 °C (5 °C steps). The results of the Li-based electrolyte were thus compared with that of the Na-based electrolyte at the same temperature and concentration conditions.

The AEM calculations were also used for the optimization of a 1 M $NaPF_6$ in $EC_x : PC_{1-x}$ (w/w) electrolyte by analysis of the conductivity as function of temperature and EC mass fraction (x). The choice of the salt concentration is based on the fact that most prototype SIBs are using this concentration. The AEM conductivity results were therefore analyzed at temperatures of −10, 30 and 50 °C and x was varied from 0.3 to 0.8 in steps of 0.05.

Using AEM data and experimental data from independent literature studies [7,8], the factors that contribute to different EC-based binary and ternary electrolytes having poor reversible capacity on hard carbon (HC) electrodes were further investigated. The binary solvents include: $EC_{0.5} : PC_{0.5}$, $EC_{0.5} : DMC_{0.5}$, $EC_{0.5} : DME_{0.5}$ and $EC_{0.5} : DEC_{0.5}$, while the ternary solvents include: $EC_{0.45} : PC_{0.45} : DMC_{0.1}$, $EC_{0.4} : PC_{0.4} : DMC_{0.2}$, $EC_{0.4} : PC_{0.4} : DME_{0.2}$ and $EC_{0.4} : PC_{0.4} : DEC_{0.2}$. In this investigation, 1 M $NaClO_4$ salt was selected from the AEM library, in order to match the conditions in the respective literature studies. The objective is to determine if the HC reversible capacity can be correlated to the amount of EC in the various electrolyte blends. Therefore, the reversible capacity of HC reported in literature was correlated to the mass fraction, volume fraction, mole fraction, and the cationic preferential ion solvation (PIS) of EC in different electrolytes.

4. Results and discussion

4.1. Comparison between experimental data and AEM results

The conductivity and viscosity results are listed in Table 1 and Table 2, respectively. Fig. 3a and b shows the conductivity and viscosity results of the $EC_{0.5} : PC_{0.5}$ (w/w) electrolyte as a function of concentration and temperature, respectively. The conductivity of the electrolyte increases with increasing $NaPF_6$ concentration in dilute electrolyte

Table 1
Conductivity experimental results for the $NaPF_6$ in $EC_{0.5}$: $PC_{0.5}$ (w/w) electrolyte at various temperatures and $NaPF_6$ concentrations.

Concentration (mol kg^{-1})	Conductivity (mS cm^{-1}) at the indicated temperature (°C)						
	−10	0	10	20	30	40	50
0.15	1.53	2.11	2.73	3.36	4.04	4.71	5.40
0.5	2.62	3.66	4.86	6.03	7.20	8.41	9.75
1	2.70	4.11	5.57	7.18	8.83	10.48	12.2
1.5	2.52	3.55	5.27	7.03	8.61	10.7	12.5
2	1.35	2.48	3.96	5.69	7.60	9.65	11.7

Table 2
Viscosity experimental results for the $NaPF_6$ in $EC_{0.5}$: $PC_{0.5}$ (w/w) electrolyte at various temperatures and $NaPF_6$ concentrations.

Concentration (mol kg^{-1})	Viscosity (cP) at the indicated temperature (°C)						
	−10	0	10	20	30	40	50
0	6.23	4.65	3.59	2.90	2.36	1.94	1.63
0.15	7.67	5.52	4.16	3.30	2.64	2.15	1.77
0.5	10.3	7.35	5.52	4.34	3.46	2.88	2.42
1	17.0	12.4	8.73	6.85	5.21	4.09	3.32
1.5	38.0	22.2	14.4	10.1	7.60	5.80	4.54
2	76.2	39.4	23.3	16.3	11.1	8.04	6.05

solutions (Fig. 3a). However, in concentrated electrolytes, the conductivity levels off and even decreases at high concentrations. This is related to a concomitant increase in several counteracting effects, such as electrolyte viscosity, ion-ion associations and the coordinated ion solvation shells [13]. Therefore, the conductivity attains a maximum at a molality of about 1 mol kg^{-1}. The electrolyte viscosity, on the other hand, is shown to increase exponentially with increasing salt concentration (Fig. 3b). Sharp increases in viscosity are found at low temperatures.

The AEM results shown in Fig. 3 are close to the experimental results over the full concentration and temperature range studied. Errors in the experimental conductivity measurements, represented by the error bars, were calculated based on the following analytical approximation [26].

$$\kappa(c,T) = K_{1,T}\, c^3 + K_{2,T}\, c^{3/2} + K_{3,T}\, c\,, \qquad [5]$$

where κ is the electrolyte conductivity [S m^{-1}], c the electrolyte concentration [mol kg^{-1}] and $K$is a temperature-dependent coefficient given by

$$K_{i,T} = K_{i,25\,^\circ C} \exp\left(\frac{E_{a,i}}{R}\left(\frac{1}{298.15} - \frac{1}{T}\right)\right),\ i = \{1,2,3\} \qquad [6]$$

where $E_{a,i}$ is the activation energy [J K^{-1} mol^{-1}] of the i^{th} temperature-dependent coefficient, R the universal gas constant [8.314 J K^{-1} mol^{-1}] and T is the temperature [K]. This model has been previously applied to experimental conductivity data of lithium-ion batteries [26]. Eqs. (5) and (6) result in an analytical expression for the conductivity at various concentrations and temperatures, which is useful in battery modeling applications. A maximum conductivity uncertainty of ±4 % was obtained at 50 °C and 2 mol kg^{-1} in the experiments.

Uncertainties in viscosity measurements were similarly calculated based on deviations from the Arrhenius expression [27].

$$\mu = \mu_\infty \exp\left(\frac{E_a}{RT}\right), \qquad [7]$$

where μ is the dynamic viscosity [Pa s], μ_∞ the limiting viscosity at infinite temperature [Pa s], and E_a is the activation energy [kJ mol^{-1}]. A maximum viscosity uncertainty of ±7 % was obtained at −10 °C and 2 mol kg^{-1} in the experiments. The uncertainties in viscosity at higher

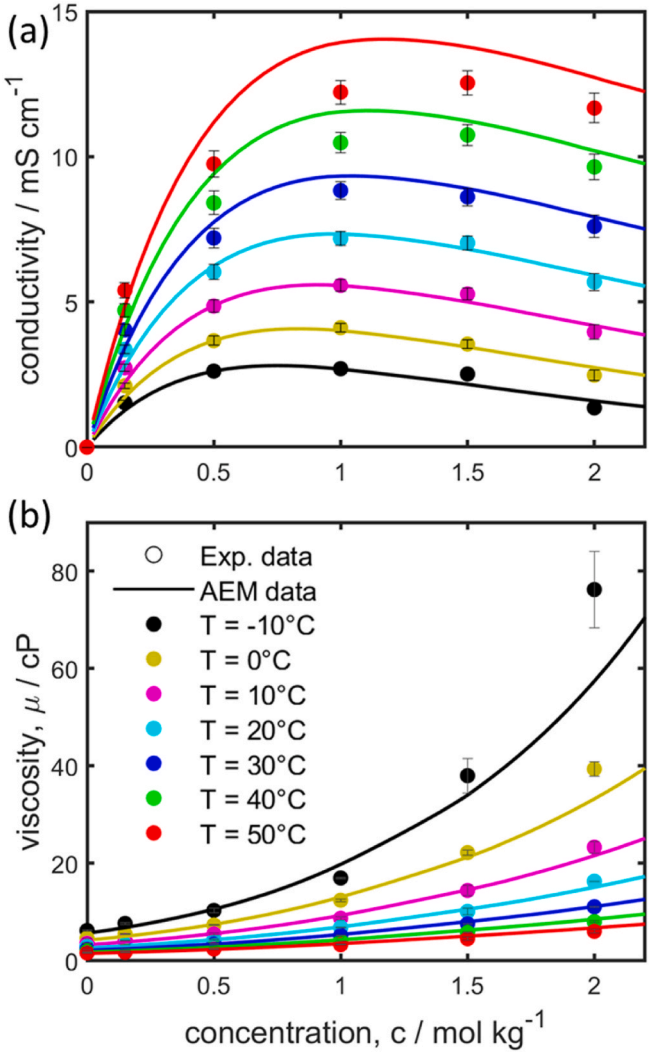

Fig. 3. Comparison of the conductivity (a) and viscosity (b) in the experiments (symbols) and AEM simulations (lines) of $EC_{0.5}$: $PC_{0.5}$ (w/w) electrolytes at various temperatures and $NaPF_6$ concentrations. The error bars are calculated from standard deviation from analytical equations.

temperatures were less than ±2 %. Alternatively, the viscosity as a function of concentration can be modeled by the Jones-Dole equation [28–30], which can be similarly applied to determine uncertainties. The resulting uncertainties are represented by the error bars on the experimental data points in Fig. 3.

Fig. 4a and b shows the analysis of the mean absolute error in conductivity and viscosity between the AEM and experimental data as a function of concentration and temperature, respectively. It can be concluded that the absolute error in conductivity is more or less constant within 1 mS cm^{-1} (Fig. 4a), and tends to increase somewhat with increasing temperature (Fig. 4b). In contrast, the absolute error in electrolyte viscosity increases substantially with increasing the $NaPF_6$ concentration (Fig. 4a) and decrease with increasing temperature (Fig. 4b). In general, deviations between the AEM simulations and viscosity experiments are the highest at the lowest temperature of −10 °C and at the highest concentration of 2 mol kg^{-1}.

Fig. 4c and d shows the mean relative error in conductivity and viscosity between the AEM and experimental data as a function of concentration and temperature, respectively. The relative error is highest at the concentration extremes (0.15 and 2 mol kg^{-1}) and temperature extremes (−10 and 50 °C). The maximum relative error of 15% is recorded for the conductivity at the lowest concentration of 0.15

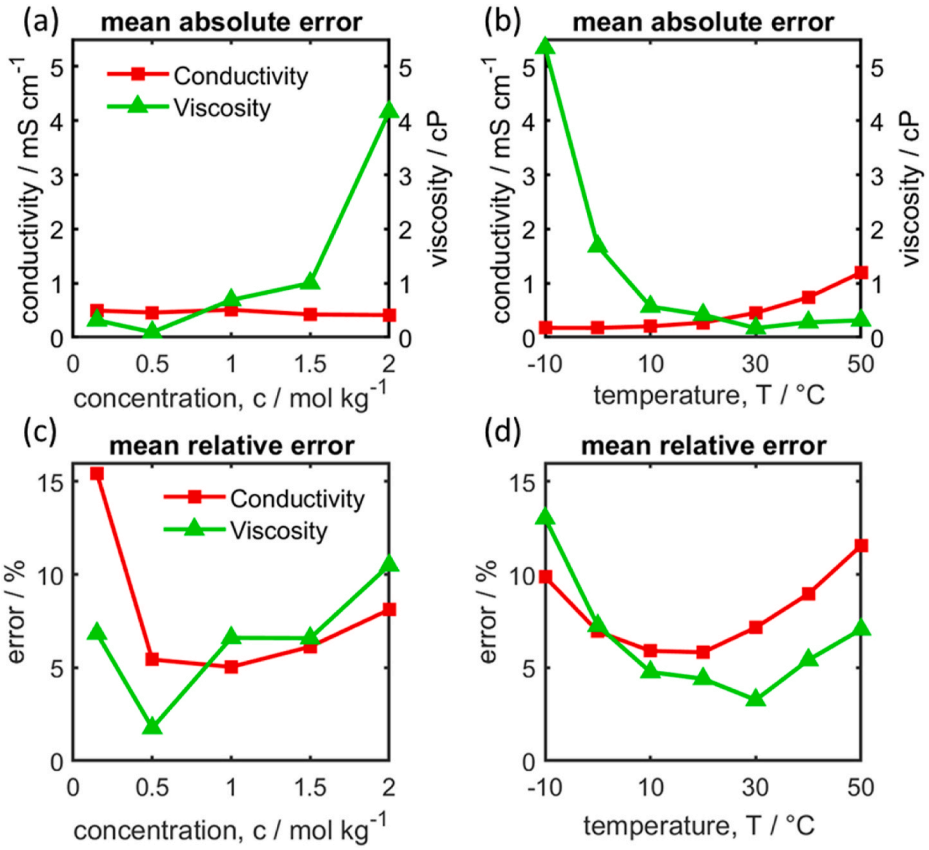

Fig. 4. Mean absolute error and relative error of the conductivity (red) and viscosity (green) between the experiments and AEM simulations at various concentrations and temperatures. Mean absolute error (a) and (b). Mean relative error (c) and (d). Mean calculated over all temperature points in (a) and (c). Mean calculated over all concentration points in (b) and (d). (For interpretation of the references to color in this figure legend, the reader is referred to the Web version of this article.)

mol kg^{-1}. At all other intermediate temperature and concentration conditions, the mean relative error in viscosity and conductivity is less than 10%, which is quite accurate and shows improvement from previous versions of the AEM [31].

4.2. Walden analysis

The relationship between the ionic conductivity and viscosity has been shown to follow a simple Stokes' law in previous investigations of ionic liquids [32] and aprotic LIB electrolytes [33]. Herein, we investigate if a similar relationship can be obtained based on experimental and AEM results of SIB electrolytes. Using Stokes' law, the ionic conductivity is expressed as a function of the electrolyte viscosity and ionic radius, as

$$\sigma = \sum_i \frac{z_i^2 F c_i^*}{6\pi\mu r_i} \quad , \qquad [8]$$

where z_i is the charge, F is the Faraday constant 96485 [c mol^{-1}], c_i^* is the molar concentration [mol l^{-1}] and r_i is the Stokes' radius of the i^{th} ionic species [m]. r_i represents the effective solvated ion radius, including the solvation shell, for ionic conductivity [11]. Considering a monovalent salt such as $NaPF_6$, Eq. (8) can be expressed as

$$\sigma = \frac{F c_\pm^*}{6\pi\mu}\left(\frac{1}{r_+} + \frac{1}{r_-}\right) , \qquad [9]$$

where r_+ and r_- are the Stokes' radii of the cations and anions, respectively, and $c_\pm^*$ is the molar concentration of dissociated cations or anions in the electrolyte. The electroneutrality condition for a monovalent electrolyte stipulates equality of ionic concentrations for oppositely charged ions. Note that, $c_\pm^*$ is only equal to the salt concentration for a fully dissociated electrolyte.

Assuming the Stokes' radii to remain constant and the salt to be either fully dissociated or the degree of dissociation to be constant, Eq. (9) can be simplified to

$$\Lambda = \frac{\sigma}{c_\pm^*} = \frac{\beta}{\mu} \quad , \qquad [10]$$

where Λ is the molar conductivity [S $cm^2 mol^{-1}$] and β is a constant which is inversely proportional to the Stokes' radii. According to Eq. [10], plots of Λ *versus* $1/\mu$ are linear. This theoretical expression has been validated experimentally in ideal electrolyte solutions according to Walden rule [32,34].

$$\log(\Lambda) = \log\left(\frac{1}{\mu}\right) . \qquad [11]$$

Eq. (11) has been experimentally validated using 1 M KCl solutions, which is assumed to represent a fully dissociated, ideal electrolyte solution [32]. The KCl data are therefore used as a reference in the present experiments to assess the ionicity or degree of dissociation of an electrolyte.

Fig. 5a and b shows the molar conductivity as a function of the inverse of the viscosity (Eq. (10)) and the Walden plot (Eq. (11)), respectively. The experimental data (colored symbols) are grouped by concentration (solid lines) while colored dots illustrate the various temperatures. In Fig. 5a, the AEM predicted Walden dependency (dashed line) matches the experimental data very well in all cases. This is another illustration of the accuracy of the AEM approach in predicting experimental data. The AEM uses a revised form of Stokes' law, which accounts for additional effects omitted by the simple Stokes' law. That form includes solvent-ion effects, ion association effects, counter-ion

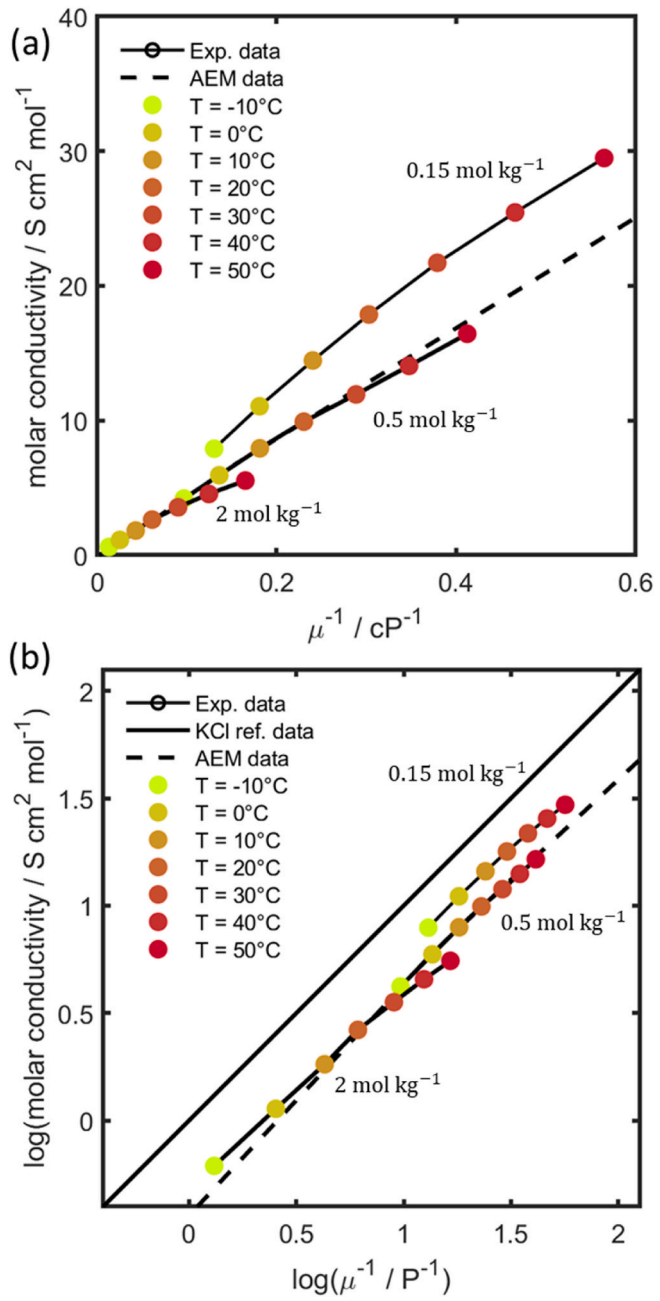

Fig. 5. Walden analysis for $NaPF_6$ in $EC_{0.5}$: $PC_{0.5}$ (w/w) SIB electrolyte. (a) Molar conductivity *versus* the inverse of the viscosity. (b) Walden plot showing the logarithmic of the molar conductivity *versus* the inverse of the viscosity. The experimental data are shown as colored dots; lines are used to group electrolytes of the same molality, and AEM modeling is represented by the dotted line. The KCl reference data line is shown in (b).

diffusion, random motion of ions, ionic hopping, viscosity as a function of salt concentration, and solvated ion size as a function of salt concentration [12]. Comparing the AEM results and the simple Stokes' law therefore reveals the extent to which these additional effects influence ionic conductivity.

Fig. 5b shows a comparison of the experimental data (colored dots), the AEM data (dashed line) and the simple Stokes' law, which is represented by the KCl reference data (solid black line). The simple Stokes' law is also shown to be a reasonable approximation of the experimental conductivity as a function of the viscosity for the electrolyte. Nevertheless, the experimental and AEM data lie below the KCl line. Points above the KCl line are characteristic of highly ionic solutions (superionic conductors) while points below the KCl line are typical for poor ionic conductors [35]. Therefore, the ionic conductivity of the $EC_{0.5}$: $PC_{0.5}$ electrolyte is less than ideal. It is worth highlighting that using the Walden rule in a rigorous interpretation of electrolyte temperature or solvent-composition dependence has been questioned [36]. Nevertheless, the empirical rule provides a facile and qualitative assessment of the degree of dissociation in electrolytes in comparative studies [37].

Because the AEM and experimental results at concentrations 0.15, 0.5 and 2 mol kg^{-1} are approximately linear and close to the KCl line, the additional effects of the revised Stokes' law do not have a large influence on the conductivity of the $EC_{0.5}$: $PC_{0.5}$ electrolyte. This means that viscosity, as predicted by the Stokes' law, has a greater influence on the electrolyte conductivity as compared to ion solvation effects. The characteristic drop in conductivity at concentrations above 1 mol kg^{-1} $NaPF_6$ in Fig. 3a is therefore primarily caused by the increase in electrolyte viscosity.

Nevertheless, several trends of the experimental data compared to the KCl reference data can be observed from Fig. 5b. The experimental data deviates slightly further from the KCl data as the concentration and temperature increase. This indicates that non-ideal ion solvation effects increase at high concentrations and temperatures. Increased deviations at 2 mol kg^{-1} are indeed expected, since electrolytes are only fully dissociated at infinite dilution. The deviations at 50 °C can be explained by the gradual increase in the mole fraction of triple ions as the temperature increases [38]. This phenomenon is herein illustrated by the decrease in the mole fraction of single ions as the temperature increases, due to reduced electrolyte relative permittivity at higher temperatures (see Fig. 6c).

4.3. Comparison of Na-ion and Li-ion battery electrolytes

It is often reported that SIB electrolytes have a higher conductivity compared to analogous LIB electrolytes [39,40]. The AEM is herein used to investigate and compare properties of 1 M $NaPF_6$ and 1 M $LiPF_6$ in $EC_{0.5}$: $PC_{0.5}$ (w/w). Using the same solvent removes the question of the dielectric permittivity, and using salts of the same anion and concentration, allows any differences to be attributed to the charge density of the cation.

Table 3 shows a comparison of the main electrolyte properties at 25 °C determined by the AEM. The main advantages of Na-based electrolytes over Li-based electrolytes are a higher conductivity (15%), lower viscosity (−13%), higher diffusivity (14%), and better solubility, as indicated by the lower free energy of solvation (−33%). For this reason, Na-based salts can dissolve in low dielectric solvents and therefore display better ion transport properties. Other effects such as the solvated ion diameter, ion solvation numbers, and cation transference numbers have only a marginal influence (<4%). The solvated ion diameter here represents the effective transport diameter, which includes the bare-ion diameter and the hard-sphere or collision diameter [13]. Based on the ion solvation numbers, it is apparent that anions are poorly solvated. This corroborates the findings that the electrolyte conductivity is mainly influenced by solvated cations [41]. Finally, the transference numbers of the two electrolytes are almost identical due to the similarities in solvated ion size.

Fig. 6 shows AEM results comparing properties of $NaPF_6$- and $LiPF_6$-based $EC_{0.5}$: $PC_{0.5}$(w/w) electrolytes as a function of the salt concentration and electrolyte temperature. Fig. 6a, b, and c show the conductivity, viscosity, and mole fraction of single ions (SI), as a function of electrolyte concentration and temperature, respectively. A series of thermodynamic mass action law (MAL) expressions within AEM predict the equilibrium proportions of single ions, ion pairs (IP) and triple ions (TI), as well as the onset of solid solvates. MAL calculations are sensitive to the relative permittivity of the electrolyte solution, which is allowed to vary over salt concentration due to the absolute concentrations and electrostatic fields of SI, IP, and TI species. While the

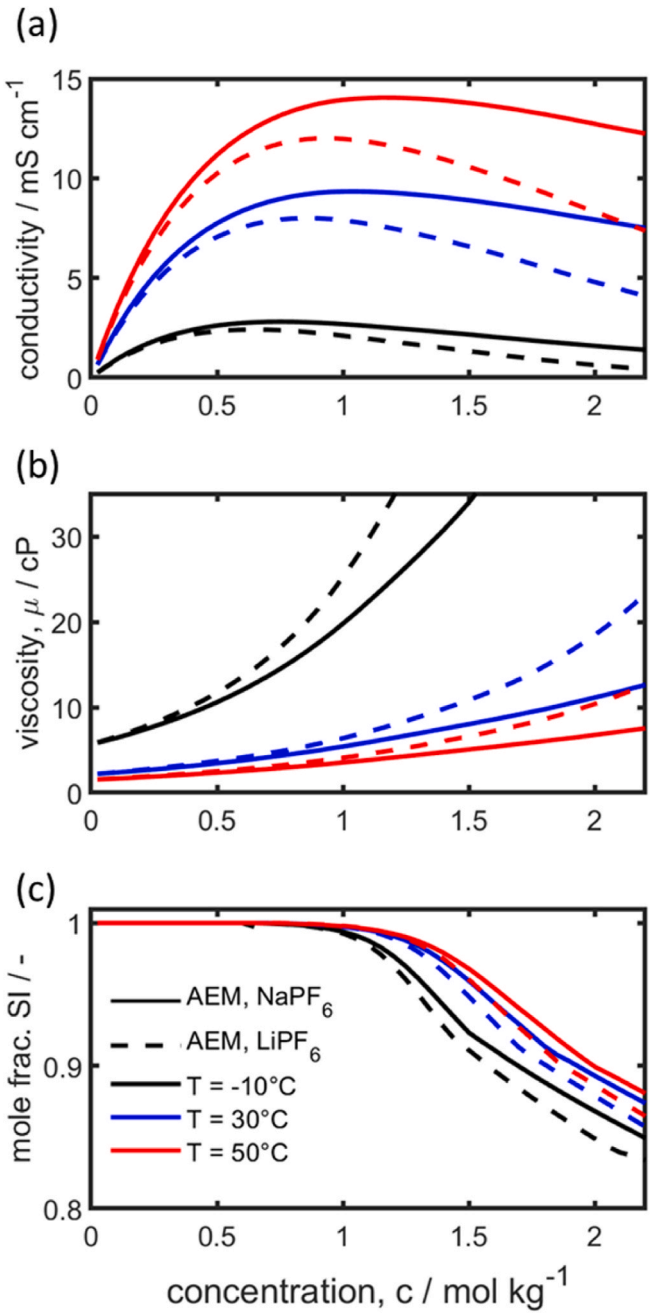

Fig. 6. Comparison of AEM simulated conductivity (a), viscosity (b) and mole fraction of single ions (SI) (c) for $NaPF_6$- (solid lines) and $LiPF_6$-based (dashed lines) electrolytes in $EC_{0.5}$: $PC_{0.5}$(w/w) at −10 (black lines), 30 (blue lines), and 50 °C (red lines) as a function of concentration (molality). (For interpretation of the references to color in this figure legend, the reader is referred to the Web version of this article.)

conductivity, viscosity, and SI values are nearly indistinguishable in (dilute) concentrations below 0.5 mol kg^{-1}, the differences between the two salts become more pronounced at higher concentrations. At concentrations above 1 mol kg^{-1}, the conductivity and the mole fraction of SI decrease more rapidly in $LiPF_6$ compared to $NaPF_6$, while the viscosity of $LiPF_6$ increases more sharply compared to that of $NaPF_6$. This drop in conductivity is due in part to the 2% larger solvated cation diameter of Li^+, as shown in Table 3, which corresponds to a substantially larger solvated proportion of its diameter compared to Na^+once their bare ions are subtracted from their solvated volumes. Nevertheless, ion dissociation remains high even as the concentration exceeds 2

Table 3
Comparison of AEM-simulated electrolyte properties of 1 M $NaPF_6$and 1 M $LiPF_6$in $EC_{0.5}$: $PC_{0.5}$ (w/w) at 25 °C.

Property	$LiPF_6$	$NaPF_6$	Unit	% Difference[a]
Electrolyte conductivity	7.117	8.211	mS cm^{-1}	15.4
Electrolyte Viscosity	6.12	5.34	cP	−12.7
Effective diffusivity	1.02×10^{-10}	1.16×10^{-10}	m^2 s^{-1}	13.7
Free energy of solvation	483.17	323.23	kJ mol^{-1}	−33.1
Solvated cation diameter	7.52	7.38	Å	−1.9
Solvated anion diameter	6.41	6.35	Å	−0.9
Cation solvation number	4.244	4.065	-	−4.2
Anion solvation number	1.313	1.301	-	−0.9
Cation transference number	0.453	0.457	-	0.9

[a] Based on the formula.$([NaPF_6] - [LiPF_6])/[LiPF_6] \times 100$.

mol kg^{-1} with the mole fraction of SI above 85%. This result indicates that the dilute solution theory can be adequately applied to model most LIB and SIB electrolytes whose equilibrium concentrations are typically around 1 M.

The interesting feature on the conductivity profile of the $NaPF_6$ electrolyte is that the conductivity remains high and close to the peak at high concentrations. Na-based electrolytes, therefore, outperform analogous Li-based electrolytes at high salt concentration and low-temperature conditions. These results should encourage the exploration of highly concentrated SIB electrolytes, which have improved thermal stability, a wider electrochemical stability window, and fast electrode kinetics [18,19]. Nevertheless, the high viscosity under these conditions might present wettability challenges when using common separators.

4.4. Preferential ion solvation (PIS) – why some electrolyte combinations fail

EC is an electrolyte solvent with high dielectric permittivity which forms a stable solid electrolyte interface (SEI) on HC and graphite electrodes [42,43]. Due to these properties, EC is considered an indispensable component in mixed battery electrolytes [5]. Nevertheless, EC has a high viscosity and is a solid at room temperature, making its use as a pure solvent impossible. EC is therefore commonly found in mixed solvents containing low viscosity solvents such as PC, DMC, DME, or DEC, which results in improved electrolyte properties with respect to viscosity, conductivity, and liquidus temperature [5,6].

Several fundamental empirical studies have been performed to optimize binary and ternary mixtures of SIB electrolytes [7,8]. These studies concluded that $EC_{0.5}$: $PC_{0.5}$ (w/w) and $EC_{0.4}$: $PC_{0.4}$: $DMC_{0.1}$ (w/w) are the optimum electrolyte blends for SIB applications due to their wide ESW and the high reversible capacity of HC electrodes. The results of these studies are summarized in Table 4.

While the different electrolyte blends were prepared on the basis of equal EC solvent weight show different results on the reversible capacity of HC electrodes, it is interesting to investigate trends which arise when the EC solvent composition is expressed other units such as volume, and mole fraction. The objective is to understand if HC's reversible capacity reported in literature can be correlated to the amount of EC in the solvent blends (expressed in volumetric and mole fraction units) and whether the minimum composition of EC needed for stable electrolytes can be defined. Furthermore, the AEM provides values of the preferential ion solvation (PIS), a measure of the probability of finding a solvent

Table 4
Fractional composition of EC in 1 M $NaClO_4$ binary and ternary electrolytes at 25 °C.

Electrolyte	Composition of EC at 25 °C in different units				ESW (V vs. Na^+/Na)[b]	HC Cap. ($mAhg^{-1}$)
	Weight	Volume	Mole	Cation PIS[a]		
EC:PC	0.50	0.47	0.54	0.46	0.1 – 5.0	200[b]/300[c]
EC:DMC	0.50	0.44	0.51	0.36	0.1 – 4.8	180[b]
EC:DME	0.50	0.39	0.51	0.34	0.4 – 4.5	70[b]
EC:DEC	0.50	0.42	0.57	0.41	1.0 – 4.6	185[b]
EC : PC : $DMC_{0.2}$	0.40	0.36	0.43	0.33	-	265[c]
EC : PC : $DME_{0.2}$	0.40	0.35	0.43	0.32	-	100[c]
EC : PC : $DEC_{0.2}$	0.40	0.36	0.45	0.35	-	270[c]
EC : PC : $DMC_{0.1}$	0.45	0.42	0.48	0.39	-	310[c]

[a] Data derived from AEM v. 2.19.1.
[b] Data derived from literature: Ponrouch et al. [7].
[c] Data derived from literature: Ponrouch et al. [8].

molecule in the primary solvation shell of an ion. Due to the preferential association of different solvent molecules with a cation, the PIS number inevitably deviates from the bulk quantities (mass, volume and mole fraction) mentioned above [5]. In this study, the PIS of EC on the Na^+-cation is the most interesting quantity, which governs the amount of EC delivered by the cation onto the HC interface during ion intercalation and SEI formation. Therefore, high values of the EC PIS on the cation can be expected to improve the cycle stability on HC electrodes.

Fig. 7 shows the measured reversible capacity of HC (bar graphs), and calculated PIS (squares), EC volume fraction (diamonds), and EC mole fraction (triangles). Fig. 7a and b shows results for the binary and ternary SIB electrolyte mixtures, respectively. There is a direct correlation between the reversible storage capacity and the EC PIS in all solvent mixtures with correlation factors (R^2) of 0.92 and 0.95 for the binary and ternary solvents, respectively In addition, it can be deduced that a PIS minimum value of 0.4 is necessary for long-term cycle stability of HC.

The other quantitative measures are, however, inconsistent between binary and ternary mixtures. For example in volumetric terms, the binary and ternary R^2 value are 0.63 and 0.98, respectively, while in molar terms, the R^2 values are 0.05 and 0.90, respectively. As a result, it is impossible to define a target EC fraction on the basis of volumetric or molar properties. However, the volume fraction shows better correlation factors compared to the molar units and therefore presents a better choice for comparing different solvent mixtures when the PIS is not available.

4.5. Optimization of 1 M $NaPF_6$ $EC_x : PC_{1-x}$ electrolytes

Having specified the EC PIS minimum value, it is now possible to optimize the conductivity of 1 M $NaPF_6$ as a function of the $EC_x : PC_{1-x}$ (w/w) electrolyte composition. Note that for the 1 M $NaPF_6$ $EC_x : PC_{1-x}$ electrolyte, the EC PIS on the cation was found to be equal to the EC weight fraction. Fig. 8 shows the AEM calculated conductivity of 1 M $NaPF_6$ in $EC_x : PC_{1-x}$ (w/w) as function of the EC content fraction x at 50 (a), 30 (b), and −10 °C (c). Low amounts of EC are undesirable because they result in poor SEI formation at HC electrodes. Furthermore, ion-pairing effects increase under these conditions, due to a low dielectric permittivity, resulting in a low ionic conductivity. On the other hand, excessive amounts of EC are also unsuitable because the electrolyte conductivity is reduced by the increase in viscosity (see Fig. 6a) and also results in wettability issues with separators. The optimum composition is therefore between these extremes, a situation best illustrated at −10 °C in Fig. 8c. This figure further illustrates the importance of mixed solvents and why pure EC and PC solvents have lower conductivities compared to their mixed solvents. The optimum EC composition is therefore 0.55, 0.70 and 0.75 (w/w) at −10, 30, and 50 °C, respectively, which are all above the EC PIS minimum value of 0.4. Because the viscosity effects are more pronounced at low temperature, the optimum EC composition locus is lower at low temperatures.

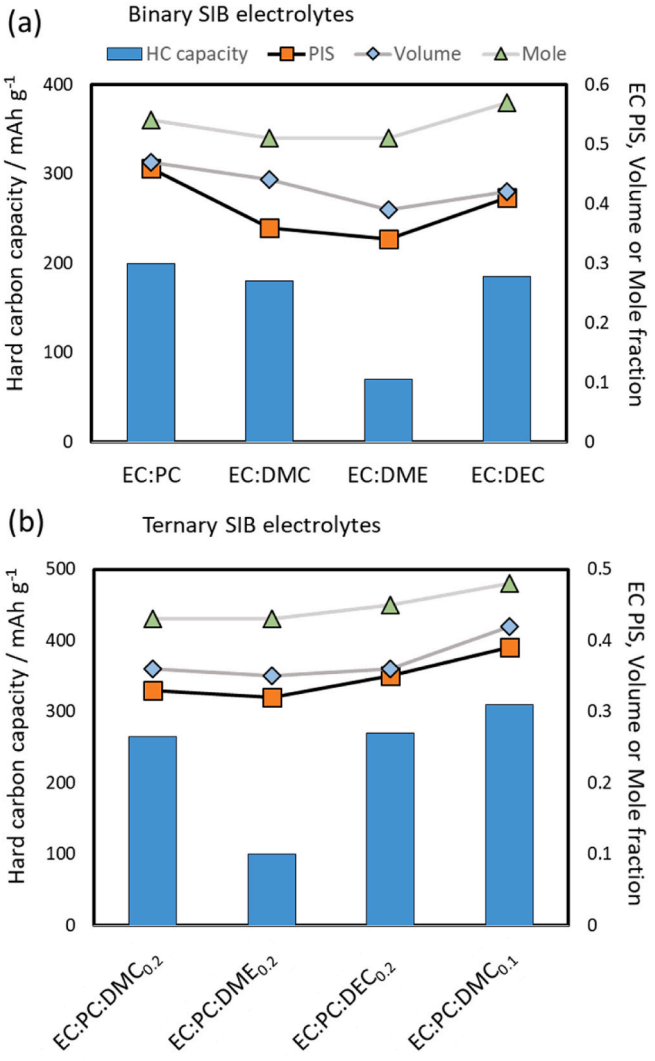

Fig. 7. Effect of EC preferential ion solvation (PIS) on the reversible capacity of hard carbon (HC) anodes for 1 M $NaClO_4$ binary (a) and ternary SIB electrolytes. HC data derived from Ponrouch et al. [7,8].

Nevertheless, the improvements in conductivity as a result of the EC composition are marginal. For example, a change in the EC weight fraction from 0.4 to 0.7 results in a 4% conductivity increase at 30 °C.

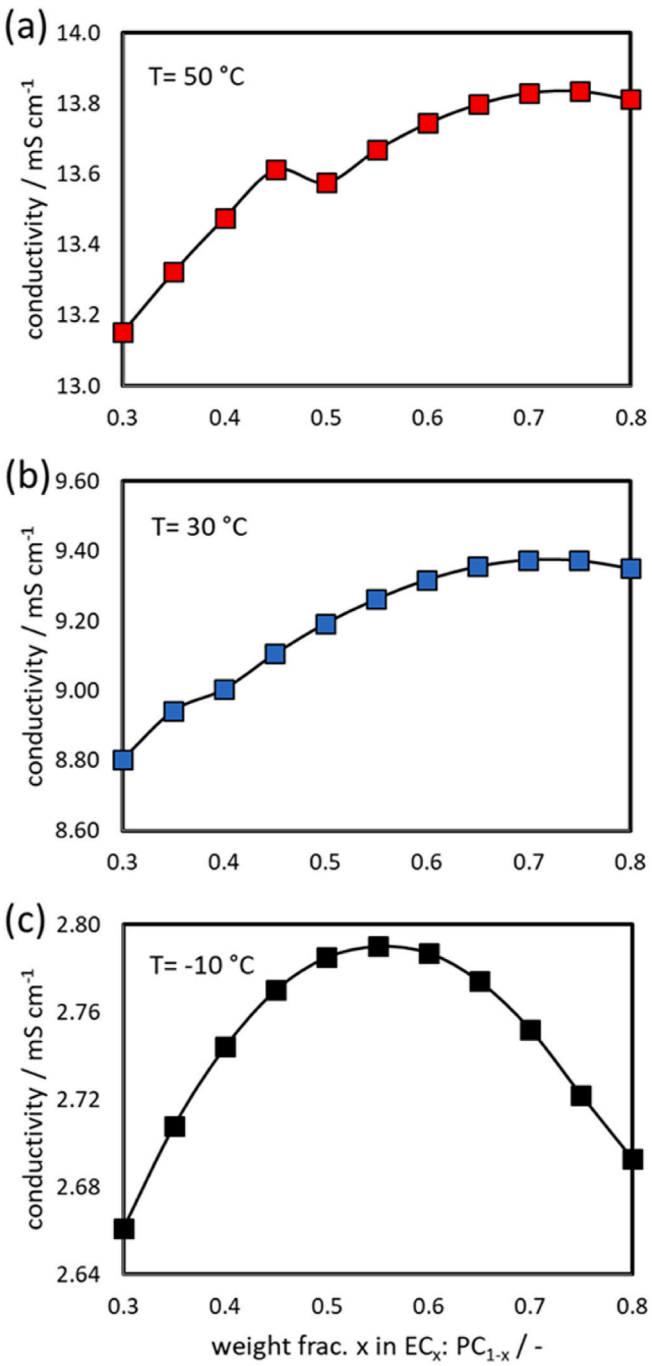

Fig. 8. Optimized AEM simulations of 1 M $NaPF_6$ EC_x : PC_{1-x} (w/w) electrolytes. Conductivity as function of EC composition x at 50 (a), 30 (b) and −10 °C (c).

There are also cost factors to consider because EC is generally the most expensive solvent. Therefore, in practice, the PIS constraint may override conductivity optimization in the final formulation.

5. Conclusions

In this work, experimental electrolyte conductivity and viscosity measurements were used in combination with the Advanced Electrolyte Model (AEM) to derive extensive properties of sodium-ion battery (SIB) electrolytes. Based on the agreement between the experimental and model data, the AEM is shown to be a reliable software to obtain extensive properties that are often difficult to measure experimentally. In addition, a method of conductivity measurement using two Pt blocking electrodes and electrochemical impedance spectroscopy (EIS) is validated and shown to be reliable for the first time in a PAT-Cell setup.

It is herein shown that the $NaPF_6$ $EC_{0.5}$: $PC_{0.5}$ (w/w) SIB electrolyte in the concentration range 0–2 mol kg^{-1} follows the simple Stokes' law, based on the Walden analysis. This implies that the electrolyte conductivity is highly dependent on the viscosity and not on ion pairing effects. This justifies the search for low viscosity, liquefied gas electrolytes, for improved battery performance at low temperatures [44]. It is further shown that 1 M $NaPF_6$ electrolyte has a 15% higher conductivity compared to the analogous 1 M $LiPF_6$ electrolyte at 25 °C, and that the conductivity of the Na-based electrolyte remains high at higher concentrations. The concentration *versus* conductivity profile of the Na-based electrolyte therefore encourages exploration of super-concentrated SIB electrolytes, with improved electrochemical stability and safety.

Finally, the optimization of the 1 M $NaPF_6$ EC_x : PC_{1-x} (w/w) electrolyte was carried out using AEM data. It is revealed that the optimized mass fraction of EC is temperature dependent and ranges between 0.55 and 0.75 at −10 and 50 °C. Using literature-derived cycling data of hard carbon (HC) electrodes, it is herein shown that the cycling stability correlates with the preferential ion solvation (PIS) of EC on the cation. Based on 8 binary and ternary electrolyte mixtures investigated, those with EC PIS on the cation below 0.4, result in poor cycle stability, which can be attributed to poor SEI formation. Given the high cost of EC, electrolyte mixture optimization might best prioritize the minimum EC PIS for stable cycling while adding a second or third low-cost and low-viscosity solvent for higher conductivity.

Future investigations will use the AEM results on conductivity, transference number and diffusion coefficient in electrochemical modeling of SIBs and will further explore the role of the EC PIS on the electrochemical stability window and reversible capacity of different carbonaceous electrodes.

Declaration of competing interest

The authors declare that they have no known competing financial interests or personal relationships that could have appeared to influence the work reported in this paper.

Acknowledgements

D.L.D. has received funding from the European Union's Horizon 2020 Research and Innovation Program under Grant Agreement No. 769900- DEMOBASE. K.C. and G.M. are grateful for the support from the European Union's Horizon 2020 Research and Innovation Program under Grant Agreement No. 646433-NAIADES.

References

[1] K. Chayambuka, G. Mulder, D.L. Danilov, P.H.L. Notten, From Li-ion batteries toward Na-ion chemistries: challenges and opportunities, Advanced Energy Materials 10 (2020) 2001310, https://doi.org/10.1002/aenm.202001310.
[2] Powerful Tiamat, Fast Charging, Enduring Cells Thanks to Sodium-Ion, 2020. http://www.tiamat-energy.com/. (Accessed 14 April 2020). accessed.
[3] J. Barker, R. Heap, N. Roche, C. Tan, R. Sayers, Y. Liu, Low Cost Na-Ion Battery Technology, Faradion Ltd, San Francisco, US, 2014.
[4] Y.-S. Hu, S. Komaba, M. Forsyth, C. Johnson, T. Rojo, A new emerging technology: Na-ion batteries, Small Methods 3 (2019) 1900184, https://doi.org/10.1002/smtd.201900184.
[5] K. Xu, Electrolytes and interphases in Li-ion batteries and beyond, Chem. Rev. 114 (2014) 11503–11618, https://doi.org/10.1021/cr500003w.
[6] K. Xu, Nonaqueous liquid electrolytes for lithium-based rechargeable batteries, Chem. Rev. 104 (2004) 4303–4418.
[7] A. Ponrouch, E. Marchante, M. Courty, J.-M. Tarascon, M. Rosa Palacín, In search of an optimized electrolyte for Na-ion batteries, Energy Environ. Sci. 5 (2012) 8572–8583, https://doi.org/10.1039/C2EE22258B.
[8] A. Ponrouch, R. Dedryvère, D. Monti, A.E. Demet, J.M.A. Mba, L. Croguennec, C. Masquelier, P. Johansson, M. Rosa Palacín, Towards high energy density sodium

ion batteries through electrolyte optimization, Energy Environ. Sci. 6 (2013) 2361–2369, https://doi.org/10.1039/C3EE41379A.
[9] Chayambuka Kudakwashe, Mulder Grietus, L. Danilov Dmitri, H.L. Notten Peter, Sodium-ion battery materials and electrochemical properties reviewed, Advanced Energy Materials 8 (2018) 1800079, https://doi.org/10.1002/aenm.201800079.
[10] E.R. Logan, E.M. Tonita, K.L. Gering, J. Li, X. Ma, L.Y. Beaulieu, J.R. Dahn, A study of the physical properties of Li-ion battery electrolytes containing esters, J. Electrochem. Soc. 165 (2018) A21, https://doi.org/10.1149/2.0271802jes.
[11] E.R. Logan, E.M. Tonita, K.L. Gering, L. Ma, M.K.G. Bauer, J. Li, L.Y. Beaulieu, J. R. Dahn, A study of the transport properties of ethylene carbonate-free Li electrolytes, J. Electrochem. Soc. 165 (2018) A705, https://doi.org/10.1149/2.0981803jes.
[12] K.L. Gering, Prediction of electrolyte conductivity: results from a generalized molecular model based on ion solvation and a chemical physics framework, Electrochim. Acta 225 (2017) 175–189, https://doi.org/10.1016/j.electacta.2016.12.083.
[13] K.L. Gering, Prediction of electrolyte viscosity for aqueous and non-aqueous systems: results from a molecular model based on ion solvation and a chemical physics framework, Electrochim. Acta 51 (2006) 3125–3138, https://doi.org/10.1016/j.electacta.2005.09.011.
[14] A.Y. Ben-Naim, Solvation Thermodynamics, Springer Science & Business Media, 2013.
[15] Y. Kuang, C. Chen, D. Kirsch, L. Hu, Thick electrode batteries: principles, opportunities, and challenges, Advanced Energy Materials 9 (2019) 1901457, https://doi.org/10.1002/aenm.201901457.
[16] J.-H. Kim, N.P.W. Pieczonka, L. Yang, Challenges and approaches for high-voltage spinel lithium-ion batteries, ChemPhysChem 15 (2014) 1940–1954, https://doi.org/10.1002/cphc.201400052.
[17] E. Berg, C. Villevieille, D. Streich, S. Trabesinger, P. Novak, Rechargeable batteries: grasping for the limits of chemistry, J. Electrochem. Soc. 162 (2015) A2468–A2475.
[18] B. Ravikumar, M. Mynam, B. Rai, Effect of salt concentration on properties of lithium ion battery electrolytes: a molecular dynamics study, J. Phys. Chem. C 122 (2018) 8173–8181, https://doi.org/10.1021/acs.jpcc.8b02072.
[19] Y. Yamada, A. Yamada, Review—superconcentrated electrolytes for lithium batteries, J. Electrochem. Soc. 162 (2015) A2406, https://doi.org/10.1149/2.0041514jes.
[20] V.M.-W. Huang, V. Vivier, M.E. Orazem, N. Pébère, B. Tribollet, The apparent constant-phase-element behavior of an ideally polarized blocking electrode: a global and local impedance analysis, J. Electrochem. Soc. 154 (2006) C81, https://doi.org/10.1149/1.2398882.
[21] M.E. Orazem, N. Pébère, B. Tribollet, Enhanced graphical representation of electrochemical impedance data, J. Electrochem. Soc. 153 (2006) B129, https://doi.org/10.1149/1.2168377.
[22] Z. Lukács, Evaluation of model and dispersion parameters and their effects on the formation of constant-phase elements in equivalent circuits, J. Electroanal. Chem. 464 (1999) 68–75, https://doi.org/10.1016/S0022-0728(98)00471-9.
[23] Gamry, Basics of EIS, Electrochemical research-impedance, n.d. https://www.gamry.com/application-notes/EIS/basics-of-electrochemical-impedance-spectroscopy/. (Accessed 19 January 2021). accessed
[24] EL-CELL - electrochemical test equipment, n.d. https://el-cell.com/. accessed March 6, 2021
[25] Anton Paar, Rheometry measuring systems, Anton Paar. (n.d.). https://wiki.anton-paar.com/en/basics-of-rheology/rheometry-measuring-systems/(accessed January 19, 2021).
[26] H. Lundgren, M. Behm, G. Lindbergh, Electrochemical characterization and temperature dependency of mass-transport properties of LiPF6 in EC:DEC, J. Electrochem. Soc. 162 (2015) A413–A420, https://doi.org/10.1149/2.0641503jes.
[27] O.O. Okoturo, T.J. VanderNoot, Temperature dependence of viscosity for room temperature ionic liquids, J. Electroanal. Chem. 568 (2004) 167–181, https://doi.org/10.1016/j.jelechem.2003.12.050.
[28] G. Jones, M. Dole, The viscosity OF aqueous solutions OF strong electrolytes with special reference to barium chloride, J. Am. Chem. Soc. 51 (1929) 2950–2964, https://doi.org/10.1021/ja01385a012.
[29] C.L. Berhaut, D. Lemordant, P. Porion, L. Timperman, G. Schmidt, M. Anouti, Ionic association analysis of LiTDI, LiFSI and LiPF 6 in EC/DMC for better Li-ion battery performances, RSC Adv. 9 (2019) 4599–4608, https://doi.org/10.1039/C8RA08430K.
[30] C.L. Berhaut, P. Porion, L. Timperman, G. Schmidt, D. Lemordant, M. Anouti, LiTDI as electrolyte salt for Li-ion batteries: transport properties in EC/DMC, Electrochim. Acta 180 (2015) 778–787, https://doi.org/10.1016/j.electacta.2015.08.165.
[31] E.R. Logan, E.M. Tonita, K.L. Gering, J.R. Dahn, A critical evaluation of the advanced electrolyte model, J. Electrochem. Soc. 165 (2018) A3350, https://doi.org/10.1149/2.0471814jes.
[32] C. Schreiner, S. Zugmann, R. Hartl, H.J. Gores, Fractional walden rule for ionic liquids: examples from recent measurements and a critique of the so-called ideal KCl line for the walden plot, J. Chem. Eng. Data 55 (2010) 1784–1788, https://doi.org/10.1021/je900878j.
[33] J.T. Dudley, D.P. Wilkinson, G. Thomas, R. LeVae, S. Woo, H. Blom, C. Horvath, M. W. Juzkow, B. Denis, P. Juric, P. Aghakian, J.R. Dahn, Conductivity of electrolytes for rechargeable lithium batteries, J. Power Sources 35 (1991) 59–82, https://doi.org/10.1016/0378-7753(91)80004-H.
[34] P. Walden, Über organische Lösungs- und Ionisierungsmittel: III. Teil: innere Reibung und deren Zusammenhang mit dem Leitvermögen, Z. Phys. Chem. 55U (1906) 207–249, https://doi.org/10.1515/zpch-1906-5511.
[35] C.A. Angell, N. Byrne, J.-P. Belieres, Parallel developments in aprotic and protic ionic liquids: physical chemistry and applications, Acc. Chem. Res. 40 (2007) 1228–1236, https://doi.org/10.1021/ar7001842.
[36] M. Nakahara, K. Ibuki, Is the Walden product useful? J. Phys. Chem. 90 (1986) 3026–3030, https://doi.org/10.1021/j100404a047.
[37] M. Dahbi, F. Ghamouss, F. Tran-Van, D. Lemordant, M. Anouti, Comparative study of EC/DMC LiTFSI and LiPF6 electrolytes for electrochemical storage, J. Power Sources 196 (2011) 9743–9750, https://doi.org/10.1016/j.jpowsour.2011.07.071.
[38] M. Valiskó, D. Boda, The effect of concentration- and temperature-dependent dielectric constant on the activity coefficient of NaCl electrolyte solutions, J. Chem. Phys. 140 (2014) 234508, https://doi.org/10.1063/1.4883742.
[39] E. Jónsson, P. Johansson, Modern battery electrolytes: ion–ion interactions in Li +/Na + conductors from DFT calculations, Phys. Chem. Chem. Phys. 14 (2012) 10774–10779, https://doi.org/10.1039/C2CP40612H.
[40] E. Flores, G. Åvall, S. Jeschke, P. Johansson, Solvation structure in dilute to highly concentrated electrolytes for lithium-ion and sodium-ion batteries, Electrochim. Acta 233 (2017) 134–141, https://doi.org/10.1016/j.electacta.2017.03.031.
[41] Y. Aihara, T. Bando, H. Nakagawa, H. Yoshida, K. Hayamizu, E. Akiba, W.S. Price, Ion transport properties of six lithium salts dissolved in γ-butyrolactone studied by self-diffusion and ionic conductivity measurements, J. Electrochem. Soc. 151 (2003) A119, https://doi.org/10.1149/1.1630592.
[42] K. Xu, U. Lee, S. Zhang, J.L. Allen, T.R. Jow, Graphite/electrolyte interface formed in LiBOB-based electrolytes : I. Differentiating the roles of EC and LiBOB in SEI formation, Electrochem. Solid State Lett. 7 (2004) A273, https://doi.org/10.1149/1.1774973.
[43] Y. Kim, K.-H. Ha, S.M. Oh, K.T. Lee, High-capacity anode materials for sodium-ion batteries, Chem. Eur J. 20 (2014) 11980–11992, https://doi.org/10.1002/chem.201402511.
[44] Y. Yang, Y. Yin, D.M. Davies, M. Zhang, M. Mayer, Y. Zhang, E.S. Sablina, S. Wang, J.Z. Lee, O. Borodin, C.S. Rustomji, Y. Shirley Meng, Liquefied gas electrolytes for wide-temperature lithium metal batteries, Energy Environ. Sci. 13 (2020) 2209–2219, https://doi.org/10.1039/D0EE01446J.